QUANTIFICATION OF GAS HYDRATES IN FRACTURED MARINE SEDIMENTS, KRISHNA GODAVARI BASIN, INDIA

By

SAMIYA AL-BULUSHI

Bachelor of Science in Petroleum Engineering

Sultan Qaboos University

Muscat, Oman

2009

Submitted to the Faculty of the
Graduate College of the
Oklahoma State University
in partial fulfillment of
the requirements for
the Degree of
MASTER OF SCIENCE
May, 2012

QUANTIFICATION OF GAS HYDRATES IN FRACTURED MARINE SEDIMENTS, KRISHNA GODAVARI BASIN, INDIA

Thesis Approved:

Priyank Jaiswal

Thesis Adviser

James Puckette

Todd Halihan

Sheryl A. Tucker

Dean of the Graduate College

.

TABLE OF CONTENTS

LIST OF TABLES

Table Page

LIST OF FIGURES

Figure Page

Figure Page

CHAPTER 1

INTRODUCTION

Natural gas hydrates are crystalline solids comprised of gas molecules bounded by cages of water molecules. They form naturally in presence of gas and water in pressure-temperature ranges nominally expected in the top few hundred meters of the seafloor on the continental shelf environments (Kvenvolden, 1994). Hydrates exhibit varied growth styles. In coarse-grained sediments they are found suspended in pore fluids (e.g., Nankai Prism; (Kida *et al.*, 2009), embedded in the rock matrix as a load-bearing component (e.g., Mackenzie Delta; Winters *et al.*, 2004), and at contacts as cement (Oseberg Field; Dvorkin and Nur, 1996). In fine-grained sediments, hydrates are found in veins (Krishna-Godavari Basin; Collett *et al.*, 2006) or massive outcrops (Gulf of Mexico; MacDonald *et al.*, 1994).

Although the potential significance of hydrates to energy and environment-related issues are well highlighted (Boswell and Collett, 2011), due to inadequate knowledge about their global volumetric changes through time, their role in changing the past climate or fulfilling the future fuel needs remain unclear. Model-based quantification methods range from empirical (Klauda, 2005) to stochastic (Davie and Buffett, 2001); these are global in nature but have a high associated uncertainty. On the other hand, data-based quantification methods mainly driven by seismic techniques range from simplistic (Wood *et al.*, 1994) to more accurate, seismic attribute

based approaches (Ecker *et al.*, 1998). These methods have lower uncertainty, but are at a basin instead off global scale. The importance of being able to quantify hydrates accurately is reflected in Dickens (2001) research who views hydrate as part of the mass balance problem in global carbon cycling.

Hydrate quantification with seismic data has been attempted in multiple ways. Generally velocity or reflectivity attributes are estimated from the seismic data, which are then related to hydrate saturation assuming simple rock models. Vargas-Cordero *et al.* (2010) used velocity estimated from pre-stack depth migration analysis to estimate hydrate growth in the pores using Biot-Gerstmann-Smith theory. Zillmer *et al.*(2005a) and Zillmer *et al.* (2005b) explained P- and S-wave velocity models from analysis of wide-aperture ocean-bottom-seismic (OBS) records with a pore-filling model implemented using the Gassmann's theory. Tinivella and Accaino (2000) used a combination of traveltime inversion and amplitude-versus-offset (AVO) analysis to simultaneously create velocity and Poission's ratio models and then relate them to hydrates in pores and grain surfaces using Gassmann's relations and percolation theory.

Although the presence of hydrates quintessentially increases the P- and S- wave velocities (V_P and V_S respectively), the rate of increase is growth-style dependent (Waite *et al.*, 2000). Dai *et al.*(2008a), Dai *et al.*(2008b) and Petersen *et al.*(2007) show that the hydrate quantification can be more accurate if these dependencies are estimated using first-principle based rock-physics methods. At a fundament level, the physical properties of a medium, such as density and elastic moduli, which determine the seismic velocities, can be computed using physical properties and relative fractions of its constituents through effective medium theory (EMT; Chand *et al.*, 2004); this includes computing the elastic moduli of dry rock matrix and pore fluid separately followed by their union through Gassman's method. Helgerud *et al.*(1999) initially developed the effective medium concept to incorporate growth of hydrates in pore spaces and within matrix.

There is a general lack of case studies where fracture-saturating hydrates are quantified using seismic and/or well data despite an abundant evidence of this growth style in nature (Daigle and Dugan, 2010b). The Krishna-Godavari (KG) basin hosts the type example of hydrate occurrence in fractures (Cook *et al.*, 2008). Imaging of 2D seismic data from the KG Basin by Jaiswal *et al.* (2012a), clearly shows a) abundance of multi-scale faults; b) patchy distribution of hydrates that are both fault and stratigraphy controlled; and c) possible presence of hydrates both in the faults as well as in the background matrix.

In this research the effective medium approach adopted by (*Helgerud et al.*, 1999) is extended to model hydrates in random dimensionless fractures. This method is then applied to the well log suite from well NGHP 01-10 to estimate gas hydrate saturation and growth styles in the matrix as well as in the fractures.

.

CHAPTER 2

METHODS

The ability of seismic data to constrain petrophysical properties of a rock depends on the predictability of its seismic response as it undergoes deformation. Thus, the relation between a changing porosity (a proxy for deformation) and the corresponding moduli (both bulk and shear; proxies for seismic response) is the basis of seismic rock physics (Wang, 2001). Two end-member relations describing porosity-moduli variation for a material can be conceived with a) incompressible pores and compressible bounding mineral grains; and b) compressible pores and incompressible bounding mineral grains (Mavko *et al.*, 2009). Mathematically, the two end-member cases can be modeled using the modified lower and upper Hashin-Shtrikman bounds respectively (Nolen-Hoeksema, 2000). Helgerud et al. (1999) showed that the relation between the elastic moduli and porosity in unconsolidated, shallow marine sediments can be appropriately described by assuming that the pores are incompressible, i.e., in a physical sense that the sediments can be conceived as inclusions within the background fluid.

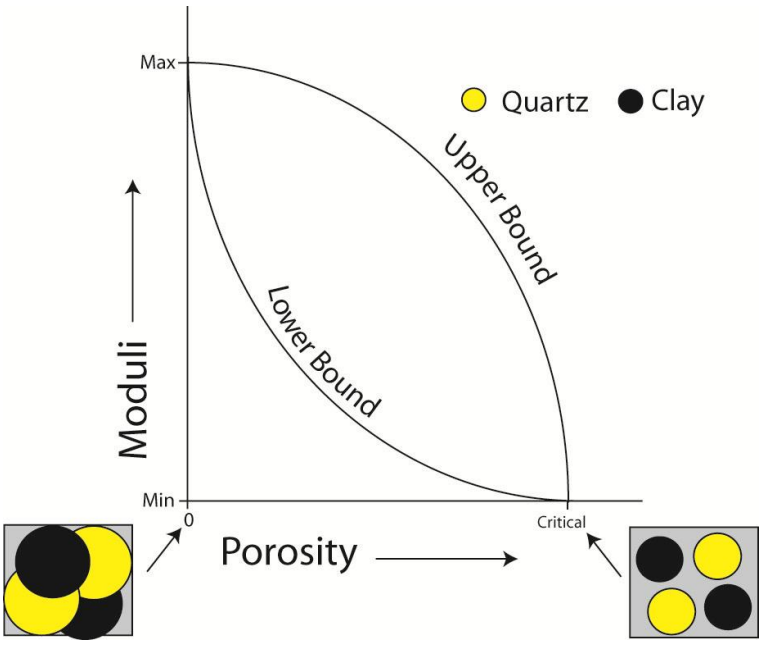

Figure 1: Porosity vs. moduli variation. In this paper, the hydrate-free rock matrix is assumed to be a 2-phase system (quartz and clay). Elastic moduli can vary with porosity in two extreme manners (upper and lower bounds), but converge at zero and critical porosity (see text for details).

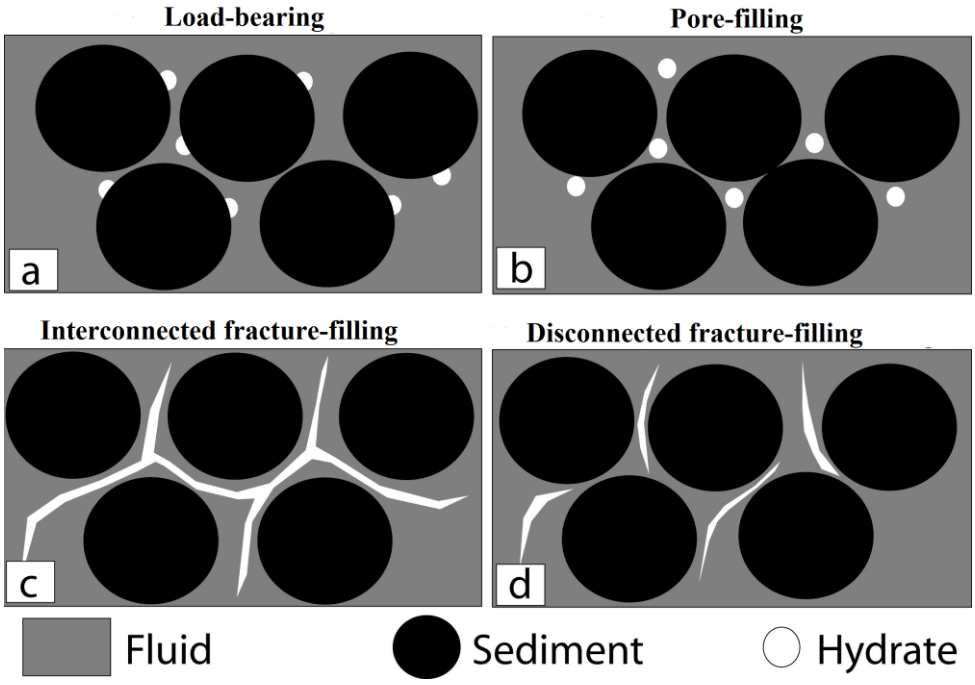

Figure 2: Cartoon of hydrate growth styles used in this paper: (a) load-bearing; (b) pore-filling; (c) interconnected; and (d) disconnected fracture-filling. In (a) - (d) mineral grains are black, fluid is grey, and hydrate is white.

2.1 Hydrate Growth in Matrix or Pore-Spaces of Marine Sediments

The bulk (K_{HM}) and shear (G_{HM}) moduli of dry, randomly packed, spherical grains at critical porosity[1] are expressed as (Helgerud *et al.*, 2000):

$$K_{HM} = \left[\frac{n^2(1-\phi_c)^2 G^2}{18\pi^2(1-\nu)^2} P \right]^{\frac{1}{3}}, \qquad G_{HM} = \frac{5-4\nu}{5(2-\nu)} \left[\frac{3n^2(1-\phi_c)^2 G^2}{2\pi^2(1-\nu)^2} P \right]^{\frac{1}{3}}. \tag{1}$$

In equation 1, n is the average number of contacts per grain, ϕ_c is the critical porosity, P is the effective pressure (difference between the pore pressure and the overburden pressure), and ν and G are the Poisson's ratio and shear modulus of the solid phase. The model described by Equation 1 is applicable to a single grain mineral packed at the critical porosity, thus providing the elastic moduli at this high-porosity endpoint (Figure 1). The other endpoint, at zero porosity (Figure 1) can be calculated for two or more mineral phases using Hill's average (Hill, 1952) and mass balance as:

$$K_s = 0.5 \cdot [\sum_{i=1}^{m} f_i K_i + (\sum_{i=1}^{m} f_i / K_i)^{-1}]; \quad G_s = 0.5 \cdot [\sum_{i=1}^{m} f_i G_i + (\sum_{i=1}^{m} f_i / G_i)^{-1}]; \quad \rho_s = \sum_{i=1}^{m} f_i \rho_i \tag{2}$$

In Equation 2, K_s, G_s, and ρ_s are the bulk and shear moduli and density of the rock matrix respectively; m is the number of the mineral components in the matrix; f_i is the volumetric fraction of the i-th component in the matrix; and K_i, G_i, and ρ_i are the bulk moduli, shear moduli and density of the i-th mineral component respectively. Bulk and Shear elastic moduli of the dry frame for $\phi < \phi_c$, are calculated using the modified lower Hashin-Shtrikman bound as:

$$K_{Dry} = [\frac{\phi_{eff}/\phi_c}{K_{HM} + \frac{4}{3}G_{HM}} + \frac{1-\phi_{eff}/\phi_c}{K_s + \frac{4}{3}G_{HM}}]^{-1} - \frac{4}{3}G_{HM}; \quad G_{Dry} = [\frac{\phi_{eff}/\phi_c}{G_{HM} + Z} + \frac{1-\phi_{eff}/\phi_c}{G_s + Z}]^{-1} - Z;$$
$$Z = \frac{G_{HM}}{6}\left(\frac{9K_{HM} + 8G_{HM}}{K_{HM} + 2G_{HM}}\right) \tag{3}$$

[1] Mineral grains become suspended in pore fluid at porosity higher than this.

In equation 3, ϕ_{eff} is the porosity associated with hydrate growth: when hydrate growth occurs in the pores, ϕ_{eff} remains constant regardless of the hydrate saturation (S_h). On the other hand, hydrate growth in the matrix as a load-bearing component can actually be seen as growth of an additional mineral phase that reduces porosity as:

$$\phi_{eff} = \phi_t (1 - S_h) \tag{4}$$

In equation (4), ϕ_t is the initial porosity with no associated hydrates.

The moduli for saturated rock can be then expressed as:

$$K_{Sat} = K_s \frac{\phi_{eff} K_{Dry} - (1+\phi_{eff}) K_f K_{Dry} / K_s + K_f}{(1-\phi_{eff}) K_f + \phi_{eff} K_s - K_f K_{Dry} / K_s}, G_{Sat} = G_{Dry}, \tag{5}$$

In equation (5), K_f is the bulk modulus of the pore-fluid. The composition of the pore fluid is assumed to be that of saline water (40000 ppm). Although hydrate growth is associated with salinity change (Liu and Flemings, 2007), for simplicity in modeling a constant fluid salinity is assumed.

When hydrates grow in the matrix (Figure 2a), the bulk modulus of the pore-fluid remains same as that of the brine ($K_f = K_w$ in Equation 5, where K_w is the bulk modulus of brine). However, when hydrates grow in pore spaces (Figure 2b), the pore-fluid bulk modulus changes with hydrate saturation as:

$$K_f = \left[\frac{S_h}{K_h} + \frac{(1 - S_h)}{K_w} \right]^{-1} \tag{6}$$

The elastic-wave velocities, V_P and V_S, can then be computed as:

$$V_P = \sqrt{\frac{K_{Sat} + \frac{4}{3} G_{Sat}}{\rho_b}} \quad ; \quad V_S = \sqrt{\frac{G_{Sat}}{\rho_b}} \tag{7}$$

In equation 7, ρ_b is the bulk density of the saturated rock expressed as:

$$\rho_b = (1-\phi_{eff})\rho_s + \phi_{eff}\rho_f \quad (8)$$

In equation 8, ρ_s and ρ_f are densities of solid and fluid phases respectively. In the load-bearing case, presence of hydrates are accounted for while calculating ρ_s (Equation 2) and ρ_f is the same as ρ_w, where ρ_w is the bulk density of brine. In the pore-filling case, ρ_s calculation only includes quartz and clay and ρ_f is computed as:

$$\rho_f = S_h\rho_h + (1-S_h)\rho_w \quad (9)$$

In Equation 9, ρ_h is the density of hydrates. The values of K_w and ρ_w are calculated using the empirical relations analytically established by (Batzle and Wang, 1992) assuming pore pressure of 12 MPa and temperature of 5 $^{\circ}$C.

2.2 Hydrate Growth in Fractures.

We model the host-sediments as an unconsolidated system wherein, assuming perfectly elastic pores and spherical grains, the porosity-modulus relation follows the modified lower Hashin-Shtrikman (HS) bounds [*Hashin and Shtrikman*, 1963]. Hydrate-saturated fractures can be modeled in two styles: – connected (Figure 2c) and disconnected (Figure 2e). "Disconnected" is intend to imply an inclusion style, and "interconnected" is intended to imply that the fractures can act like a background medium in which saturated sediments can be considered as inclusions. The porosity – moduli relation of disconnected and interconnected systems can be addressed respectively by lower and upper HS bounds (annotated "HS-" and "HS+", respectively hereafter [*Berryman*, 1995]). The upper HS bound (HS+), assumes that seismically induced pressure does

not change the pore shapes, but rather flushes the fluid in-and-out of the pore spaces while the lower HS bound (HS-) assumes that pores are perfectly elastic void spaces.

In general, the moduli (M^{HS}) of the sediment-hydrate composite can be expressed as:

$$M^{HS-/+} = K^{HS-/+} + (4/3)G^{HS-/+} \tag{10}$$

In equation (10), $K^{HS-/+}$ and $G^{HS-/+}$ are the bulk and shear moduli of the disconnected and interconnected system, respectively estimated as:

$$\begin{aligned} K^{HS(-/+)} &= \left[\sum_{i=1}^{m} \frac{f_i}{K_i + \frac{4}{3}G_{(\min/\max)}}\right]^{-1} - \frac{4}{3}G_{(\min/\max)}; \\ G^{HS(-/+)} &= \left[\sum_{i=1}^{m} \frac{f_i}{G_i + Z_{(\min/\max)}}\right]^{-1} - Z_{(\min/\max)}; \\ Z_{(\min,\max)} &= \tfrac{1}{6}G_{(\min/\max)}\left(\frac{9K_{(\min/\max)} + 8G_{(\min/\max)}}{K_{(\min/\max)} + 2G_{(\min/\max)}}\right); \end{aligned} \tag{11}$$

In Equation 11, m is the number of the mineral components. f_i is volume fraction of the i^{th} component in the mineral frame and K_i and G_i are the bulk and the shear moduli of i^{th} component respectively. Subscripts *min* and *max* refer to the minimum and maximum bulk and shear moduli of the constituents. For example, in a mixture of quartz ,clay, hydrates and brine, using Equation 11, K_{min} and G_{min} will be 2.37 GPa and 0 GPa corresponding to brine and K_{max} and G_{max} will be 36 Gpa and 45Gpa corresponding to quartz (Table 1).

V_P and V_S for the disconnected and interconnected systems are given by:

$$V_P^{D/I} = \sqrt{\frac{M^{HS-/+}}{\rho_b}}; \qquad Vs^{D/I} = \sqrt{\frac{G^{HS-/+}}{\rho_b}} \tag{12}$$

Where the bulk density (ρ_b) is now expressed as:

$$\rho_b = (1-\phi_r).\rho_m + \phi_r.\rho_c \quad (13)$$

In equation (13), ϕ_r is the fracture porosity, ρ_m is the bulk density of background computed using Equation 8, and ρ_c is the density of fracture-filling material. In this work, fractures are viewed as void spaces and therefore ϕ_r is the same as the overall volume fraction of fractures.

2.2.1 Fractures Fully Filled with Hydrates

For comparison purposes (Figure 3), we model hydrate-saturated fractures by assuming that a) sediments do not contain hydrates (in pores or matrix); b) fractures do not contain water; and c) the system is fully saturated. First, we compute the elastic moduli of water-saturated sediments using the soft rock approach of *Helgerud et al.*(2000), which assumes that dry sediments are inclusions in a fluid background by applying S_h=0 through Equations 1-9 .

When fractures are interconnected we model the system as having a softer inclusion (lower elastic moduli) in a stiffer background (higher elastic moduli) and vice versa when fractures are disconnected (Equations 10-13). Note that the computation of system elastic moduli in Equation 11 for this particular case requires three components (m = 3; Equation 11): a) a background composite of matrix and brine; b) hydrate in fractures.

In equation (13), ρ_c is the density of fracture-filling material (brine). The volume fractions of individual components in Equation 11 can be expressed in terms of ϕ_r as:

$$f_1 = 1-\phi_r \qquad f_2 = \phi_r.S_{hr} \quad (14)$$

In equation (14), f_1 and f_2 are volume fractions of background mixture and hydrate in fractures respectively and S_{hr} is the hydrate saturation in fractures, which is 100% .

For elastic velocity computation, ρ_m and ρ_c required in Equation 13 can be respectively computed as:

$$\rho_m = (1-\phi_{eff})\rho_s + \phi_{eff}\rho_w \qquad \text{and} \qquad \rho_c = \rho_h \tag{15}$$

In equation (15), symbols remain the same as in Equation 8. ρ_h and ρ_w are hydrate and brine density respectively (Table 1).

2.2.2 Fractures Partially Filled with Hydrates

The fractures are modeled assuming a partially saturated hydrate-water system. We follow the same procedure as mentioned in above section. However this time $S_h \neq 0$ in Equations 1-9.

Interconnected fractures are implemented using the upper Hashin-Shtrikman bound (Mavko *et al.*, 2009). The computation of system elastic moduli for partially saturated fractures requires three components (m = 3; Equation 11): a) a background composite of matrix and pore-fluid (hydrate can be either in matrix or in pores); b) hydrate in fractures forming an incompressible framework which includes the compressible background mixture; and c) brine in fractures.

In equation (13), ρ_c is the density of fracture-filling material (a mixture of brine and hydrate computed using equation. The volume fractions of individual components in Equation 11 can be expressed in terms of ϕ_r as:

$$f_1 = 1-\phi_r; \qquad f_2 = \phi_r \cdot S_{hr}; \qquad f_3 = \phi_r \cdot (1-S_{hr}) \tag{16}$$

In equation (16), f_1, f_2 and f_3 are volume fractions of background mixture, hydrate in fractures and brine in fractures, respectively, and S_{hr} is the hydrate saturation in fractures.

For elastic velocity computation, ρ_m and ρ_c required in Equation 13 can be computed , respectively, as:

$$\rho_m = (1-\phi_{eff})\rho_s + \phi_{eff}\rho_f \quad (17)$$

$$\rho_c = f_2.\rho_h + (1-f_2).\rho_w \quad (18)$$

In equation (17), symbols remain same as in Equation 8. In equation (18), f_2 is computed using Equation (16).

Although disconnected fractures are implemented using the lower Hashin-Shtrikman bound (Mavko *et al.*, 2009), for stability reasons we assume that brine in the disconnected fractures is part of the background matrix. The practical implementation involves decreasing the fracture porosity corresponding to the volume fraction of brine in the disconnected fractures and proportionately increasing the background porosity. As a result, the volume fractions of components in Equation 11 are recalculated as:

$$\bar{f}_2 = \phi_r - f_3; \quad \bar{f}_1 = f_1 + f_3 \quad (19)$$

In Equation 19, $\bar{f}_1$ is the fraction corresponding to the background mixture of matrix and pore-fluid (hydrates can be part of the matrix or the pore-fluid and the brine in the pore-fluid is both "in-situ" and that shifted from fractures to the background for modeling purposes); and $\bar{f}_2$ is the hydrate fraction saturating the fractures conceived as incompressible inclusions. Thus, computation of elastic moduli in the disconnected fracture case requires only the two components given in Equation 19(m = 2; Equation 11).

CHAPTER 3

APPLICATIONS AND RESULTS

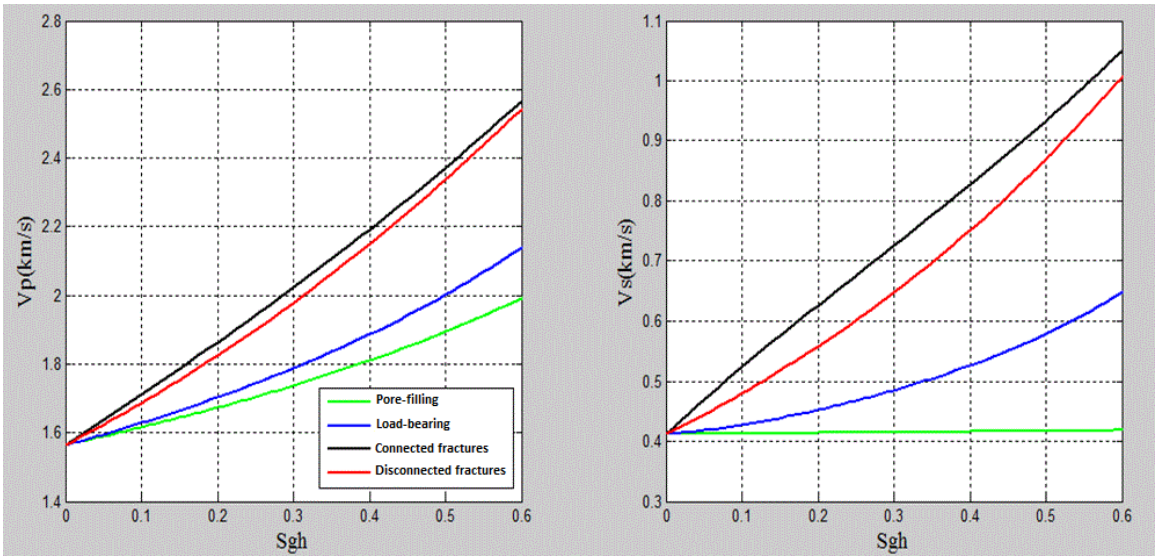

Figure 3: Sgh versus (a) VP and (b) VS for the hydrate-sediment composite. Velocity enhancement is a maximum when hydrates are in-fractures, within which the connected fractures have higher velocities.

In Figure 3 we compare the elastic velocity increase for the hydrate-sediment composite with increasing hydrate saturation (S_{gh}) for hydrate states shown in Figure 2. The model shown in Figure 3 assumes that the sediment matrix is an unconsolidated clay-quartz mixture(80% and 20% respectively) with 65% initial bulk porosity and an effective pressure of about 1.2 MPa (corresponding to ~1000m of water depth). This system is representative of fine-grained, unconsolidated, sediments within the top few hundred meters of the seafloor. Other modeling parameters are listed in Table 1. Hydrates in the load-bearing case (Figure 1a) are modeled as part of the matrix, hence, the matrix porosity gradually decreases with increasing Sgh as:

$\phi_{eff} = \phi_t(1 - S_h)$. Thus, elastic velocity increase in the load-bearing case is partly due to a gradual decrease in porosity and partly due to stiffening of dry-rock matrix (blue trend; Figure 3). In the pore –filling case (Figure 2b), hydrates are modeled as part of the background fluid increasing the V_P while maintaining relatively constant V_S (green trend; Figure 3). Introduction of fractures in natural systems increase the total porosity [*Cook et al.*, 2008]. In our modeling, the fractures can be introduced in two ways: first, leading to a total porosity increase; and second, maintaining a constant total bulk porosity by reducing the matrix porosity as fracture density is increased. We adopt the second method as is a more reasonable comparison to hydrates in load-bearing and pore-filling states. Thus, in Figure 3, $S_{gh} = 0.6$ for connected and disconnected fractures implies that 60% of the system porosity is present as fracture porosity leaving only 40% as matrix porosity.

Our strategy for hydrate quantification at the NGHP-01-10 site is first done by determining individual hydrate saturation profiles corresponding to the matrix and the fractures with the help of standard well-log suites. Collette *et al.*(2006) previously showed that at the NGHP-01-10 site: a) hydrates are present in fractures as well as in the background (matrix and/or pores); b) fractures may have random orientation; and c) sediments are unconsolidated and dominantly fine-grain. The key aspect of our application is to be able to determine the growth style of hydrates and the associated saturation at the NGHP-01-10 site such that the observed V_P, V_S, and S_h (from core-depressurization) are simultaneously predicted. The saturation and the growth styles are estimated in a trial-and-error manner through repeated forward modeling such that the overall prediction error, estimated by root-mean-square error, is within 5% of the observed data.

3.1 Computation of Background and Fracture Saturation Profile

A gross assessment of the deep and shallow resistivity log separation (Figure 4a), which is considered as a proxy for fluid invasion in sediments, suggests that the entire section comprises two rock architectures. The first architecture, such as 90 – 120m depth (Figure 4a), has no separation which is suggestive of limited fracturing. The second architecture, such as from 40 – 90m and 120 – 150m depth (Figure 4a), has clear separation, which is suggestive of significant fracturing. The porosity log (Figure 4b), computed from the density log, shows that fracture limited architecture has a consistent porosity of ~55% while the fractured architecture has variable and sometimes extremely high porosity estimates. For modeling purposes we consider the porosity of the fracture-free architecture, 55%, as the matrix porosity (ϕ_m). Consequently, in fracture-prone architecture porosity higher than 55% is attributed to fractures (ϕ_r). Further, we assume that the maximum and minimum gamma-ray log values respectively correspond to 100% and 60% clay content; the clay profile (Figure 4c) is generated accordingly. Other modeling parameters include P = 1.2 MPa (pressure at ~1000m water depth) and a ϕ_c = 65%. Application of the modeling methodology (Chapter 2, section 1) in the fracture-free zone suggests that the observed V_P, V_S and S_h data can be best explained with 23%±2% hydrates in the matrix in a load-bearing state (Figure5). Next, in fracture-prone zones, we compute the fracture porosity (cyan curve; Figure 3b) as: $\phi_r = \phi_t - 0.55$, where ϕ_t is the observed value from the density-porosity log (pink curve; Figure 4b). We then apply the modeling methodology in chapter 2 section 2 for partially saturated fractures to estimate the elastic moduli and density of the system. We use Equations 11 – 13 to predict V_P and V_S. The total hydrates saturation (S_{ht}) prediction, which is used to compare with the observed hydrate saturation, is done as:

$$S_{ht} = \frac{\phi_m \cdot S_{hm} + \phi_r \cdot S_{hr}}{\phi_t} \tag{20}$$

In Equation 20, S_{hm} is hydrate saturation in matrix. While choosing S_{hm} and S_{hr} in a trial-and-error manner for data prediction, S_{hr} is modeled with both interconnected and connected fracture assumptions.

Within 60-90 m and 42-60 m depth (Figure 6-7) we obtain data match within 5% RMS error by assuming interconnected fractures, S_{hr} = 60%±5 and 70%±5 respectively, and S_{hm} =15±3% and 10±3% respectively. Similarly, within 25-42 depth (Figure 8) we obtain data match within 5% RMS error by disconnected fractures, S_{hr} = 90%±5, and S_{hm} = 7±3%. Within 125-150 m depth we can obtain data match within 5% RMS error with connected as well as disconnected fractures (Figures 6) possibly due to low volume fraction of fractures. Individual S_{hr} and S_{hm} profiles generated from Figures 5–8 (Figure 9) show that while hydrate saturation within the matrix increases from the seafloor towards the BSR, hydrate saturation within the fractures exhibit an inverse relationship.

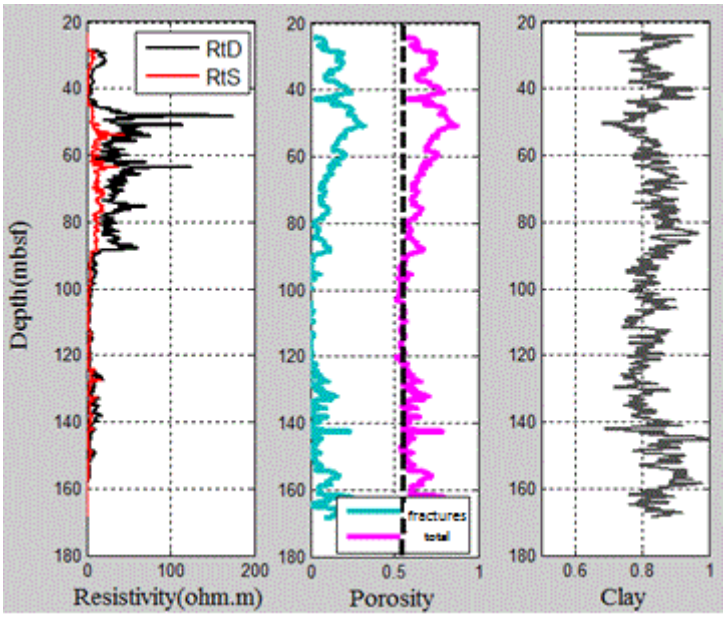

Figure 4: Wire line logs at Site NGHP-01-10. From left to right - resistivity (black indicates deep induction and red indicates shallow induction), Density porosity (pink indicates total porosity based on grain density of 2.65 g/cc and cyan indicates fractures porosity, and dashed black line indicates matrix porosity) and estimated clay content from gamma ray log

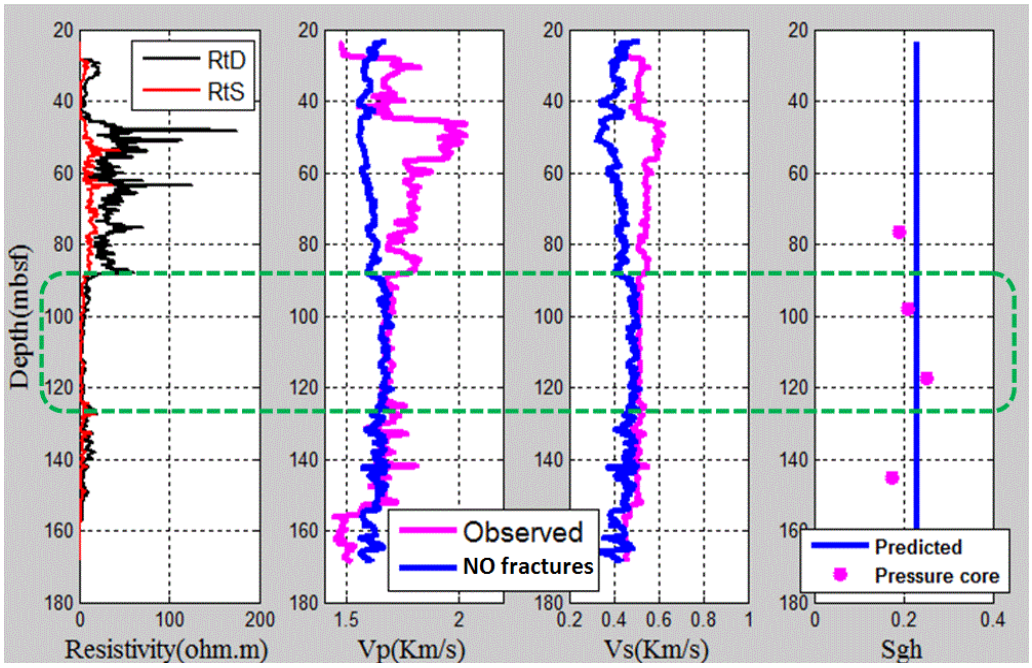

Figure 5: Fracture-free zone modeling. Dashed green box indicates the interval. Predicted trends are indicated in blue. 5% RMS prediction error in VP and VS prediction honoring the observed saturations can be obtained with 23% hydrate in the matrix as a load-bearing phase.

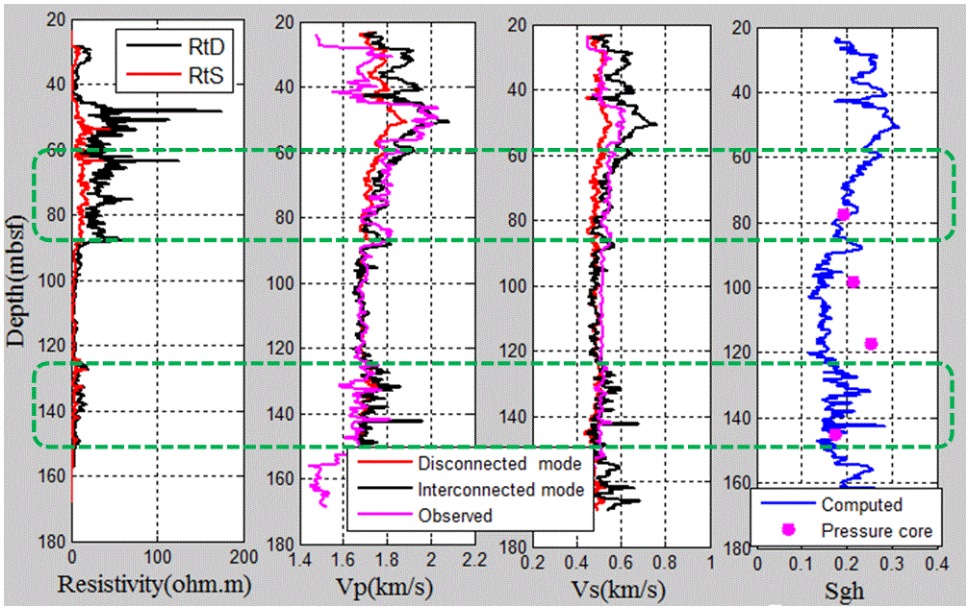

Figure 6: Fracture-prone zone modeling. Dashed green box indicates the intervals. Predicted trends are indicated in blue. 5% RMS prediction error in VP and VS prediction honoring the observed saturations can be obtained in both the interval with 15% hydrate in the matrix as a load-bearing phase and 60% hydrate in disconnected fractures.

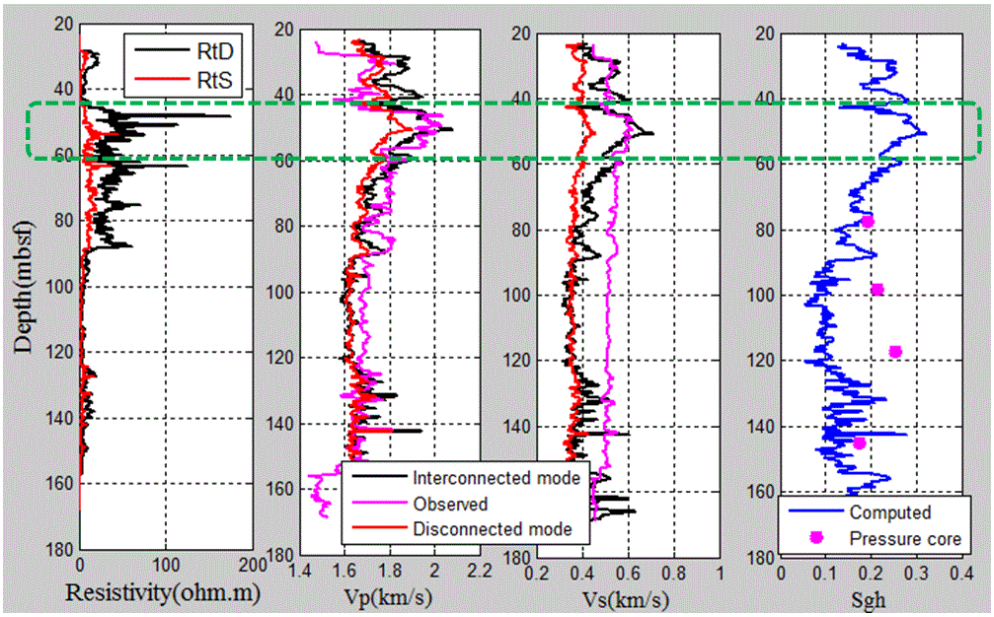

Figure 7: Fracture-prone zone modeling. Dashed green box indicates the interval. Predicted trends are indicated in blue. 5% RMS prediction error in VP and VS can be obtained with 10% hydrate in the matrix as a load-bearing phase and 70% hydrate in interconnected fractures.

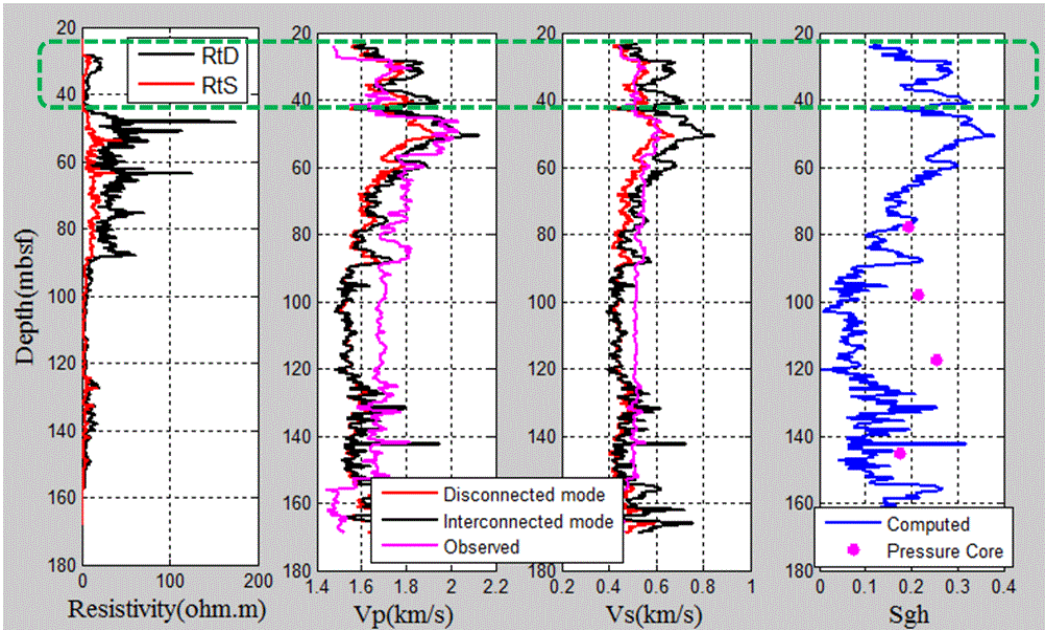

Figure 8: Fracture-prone zone modeling. Dashed green box indicates the interval. Predicted trends are indicated in blue. 5% RMS prediction error in VP and VS can be obtained with 7% hydrate in the matrix as a load-bearing phase and 90% hydrate in interconnected fractures.

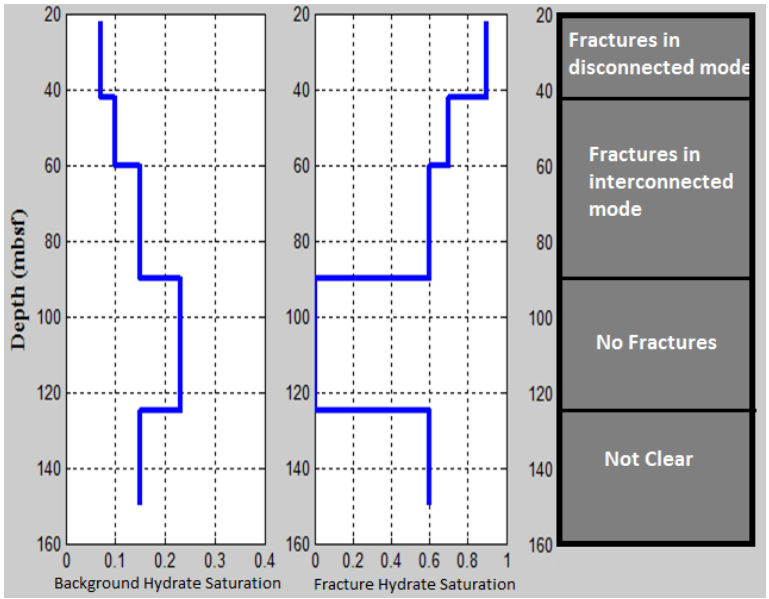

Figure 9: Hydrate Saturation profiles. Left: saturation in the matrix, and right: saturation in the fractures. Hydrates mode are indicated beside the profiles.

CHAPTER 4

DISCUSSION

The results (illustrated in Figure3) can be closely compared to [*Sava and Hardage*, 2010] who modeled the effect of hydrates in horizontal thin layers interlayered with unconsolidated marine sediments. Similar to this work, they show that when the same volume of hydrates is concentrated in thin layers as opposed to being disseminated in matrix, elastic velocities increase more rapidly. However, they also show that the system becomes more anisotropic as hydrate become concentrated in thin layers. [*Jakobsen et al.*, 2001] also show that although connected hydrates increase elastic velocities, they can increase anisotropy if grain alignment is considered. Unlike the previous studies, the fractures in this study do not necessarily have a preferred orientation and therefore are not intended to induce anisotropy. The system is treated as isotropic which could still be applicable in fine grained medium where fracture orientations are generally random.

The character of the hydrate saturation profile in the matrix (the left profile in Figure 9) can be explained using the diffusive transport model of (Bhatnagar *et al.*, 2007) which involves methanogenesis from deposition and burial of the organic matter. However, the character of the hydrate saturation profile in the fractures (the left profile in Figure 9) is non-intuitive.

Nominally, it is expected that due to the high permeability nature of the fractures diffusive flow will enable hydrate migration from the matrix into the fractures (Frederick and Buffett, 2011). Thus, if the hydrate saturation in the matrix is higher, saturation in fractures should also be higher. However this is unlike the saturation profiles in this study. We posit that hydrates in fractures in the study area are not formed due to diffusive process but rather due to advective fluid-flow channeled from below the BHSZ through preexisting faults and fractures.

Jaiswal *et al.* (2012a) suggests tectonic uplift in the vicinity of the NGHP-01-10 site. It further suggests that due to tectonic uplift hydrate will be pushed out of the stability zone followed by their dissociation into free gas and re-enters into the stability zone through fractures formed during the tectonic uplift. The re-entry, which possibly happens through focused fluid-flow, promotes hydrate precipitation in the fractures. As hydrate move out of the stability zone during the tectonic uplift and dissociate, the advecting fluids carry dissolved methane through the stability zone. As the methane solubility decreases towards the seafloor, the maximum hydrate precipitation occurs closer to the seafloor.

The fractures in our model could have originated through both shear fracturing from tectonic movement and hydraulic fracturing through hydrate occlusion (Daigle and Dugan, 2010a). Hydraulic fracturing in the study area has also been advocated by Rees *et al.* (2011). We expect that hydrate occlusion will initially create and saturate disconnected fractures which could also partly explain high hydrate saturation near the seafloor. In time, the disconnected fractures can grow to become interconnected by getting mutually coupled or getting coupled with pre-exiting shear fractures. We expect that the shear-fracture sets will be through-going and therefore actively advecting fluids. This may be the physical reasoning behind the high hydrate saturation observed in the connected fractures in our modeling (Figure 9).

The log data from site NGHP-10-10 has also been investigated by Lee and Collett (2009) and Gosh *et al.* (2010); both authors attempt to predict the observed V_P and V_S data using anisotropic modeling. While Lee and Collett (2009) introduce anisotropic propagation through fractures, Gosh *et al.* (2010) make the system anisotropic by including hydrates as vertical ellipsoids. To obtain a reasonable match (<5% prediction error) simultaneously in V_P and S_h data, Lee and Collett (2009) had to assume hydrate growth in vertical fractures. However, to obtain the same match in the observed V_S and S_h data, they had to tilt the fracture orientation closer to horizontal. Gosh *et al.* (2010) could obtain a reasonable match in both Vs and V_P data; however, the required hydrate saturation was ~50% more than the observed saturation. The fact that we could simultaneously match the observed V_P and V_S within 5% RMS prediction error honoring the observed saturation, suggests that our assumption of system being isotropic is reasonable. While we do not intend to imply that fractures cannot introduce anisotropy, their potentially random arrangement (Rees *et al.*, 2011) could have made the overall system appear isotropic to the propagating seismic waves.

Volumetric measurements of hydrates have been statistically driven based on average extent and thickness of the GHSZ, porosity, gas yield, total organic carbon, or more simply, the BSR amplitudes (Milkov, 2004). In fractured sediments, such as in the KG basin, significant volumes of hydrates exist in the fractures besides the pore-spaces. Thus, in hydrate quantification which is based on seismic velocity discounting fractures may lead to significant over-prediction of hydrates. (Boswell and Collett, 2010) suggest that $\sim 10^4$ TCF of methane could be trapped as gas hydrates in marine environments, mainly in fine-grained sediments. In general, fine-grained sediments are fracture prone. Thus, basin-wide prediction of hydrates accounting for hydrates in fractures could therefore have wider implications on their global estimates.

Table 1: Constants parameters used in the models

System Components	Density(g/cc)	Bulk Modulus (Gpa)	Shear Modulus(Gpa)
Clay	2.58	21	7
Quartz	2.65	36	45
Hydrates	0.91	7.7	3.2
Water	1.033	2.37	0

CHAPTER 5

CONCLUSIONS

This research suggests that seismic velocities (V_P, V_S) and hydrate saturation observed in the KG Basin at NGHP-01-10 site can explained by simultaneously assuming two growth styles of hydrates– in matrix as a load-bearing phase as well as in fractures in a non-load-bearing phase. We show that presence of hydrates in fractures increase V_P and V_P faster than hydrates in pore-spaces or in the matrix as a load-bearing component. The rate of increase, however, is dependent on the mode of fractures connection - interconnected fractures increase the seismic velocities faster than disconnected fractures. In the KG Basin, fractures have high (>50%) hydrate saturation. The hydrate saturation profile in the matrix shows an increase towards the bottom simulating reflector (BSR). The hydrate saturation profile in the fractures shows an increase towards the seafloor. We speculate that the hydrate saturation profile in fractures is solubility driven. We also speculate that fractures in the NGHP-01-10 site could have both shear-failure and hydraulic-fracturing origins.

REFERENCES

Berryman, J. (1995), Mixture theories for rock properties, in *American Geophysical Union Handbook of Physical Constants, ,* edited by T. J. Ahrens, AGU, New York.

Bhatnagar, G., W. G. Chapman, G. R. Dickens, B. Dugan, and G. J. Hirasaki (2007), Generalization of gas hydrate distribution and saturation in marine sediments by scaling of thermodynamic and transport processes, *American Journal of Science*, *307*, 861-900.

Bohrmann, G., J. Greinert, E. Suess, and M. Torres (1998), Authigenic carbonates from the Cascadia subduction zone and their relation to gas hydrate stability, *Geology*, *26*, 647-650.

Chand, S., T. A. Minshull, D. Gei, and J. M. Carcione (2004), Elastic velocity models for gas-hydrate-bearing sediments - a comparison, *Geophysical Journal International*, *159*(2), 573-590.

Collett, T., M. Riedel, J. Cochran, R. Boswell, J. Presley, P. Kumar, A. Sathe, A. Sethi, M. V. Lall, and V. Sibal (2006), Expedition 01 Initial Reports*Rep.*

Cook, A. E., D. Goldberg, and R. L. Kleinberg (2008), Fracture-controlled gas hydrate systems in the northern Gulf of Mexico, *Marine and Petroleum Geology*, *25*(9), 932-941.

Dai, J. C., F. Snyder, D. Gillespie, A. Koesoemadinata, and N. Dutta (2008), Exploration for gas hydrates in the deepwater, northern Gulf of Mexico: Part I. A seismic approach based on geologic model, inversion, and rock physics principles, *Marine and Petroleum Geology*, *25*(9), 830-844.

Daigle, H., and B. Dugan (2010), Origin and evolution of fracture-hosted methane hydrate deposits, *Journal of Geophysical Research-Solid Earth*, *115*.

Dvorkin, J., and A. Nur (1996), Elasticity of high-porosity sandstones: Theory for two North Sea data sets, *Geophysics*, *61*(5), 1363-1370.

Berryman, J. (1995), Mixture theories for rock properties, in *American Geophysical Union Handbook of Physical Constants, ,* edited by T. J. Ahrens, AGU, New York.

Bhatnagar, G., W. G. Chapman, G. R. Dickens, B. Dugan, and G. J. Hirasaki (2007), Generalization of gas hydrate distribution and saturation in marine sediments by scaling of thermodynamic and transport processes, *American Journal of Science*, *307*, 861-900.

Bohrmann, G., J. Greinert, E. Suess, and M. Torres (1998), Authigenic carbonates from the Cascadia subduction zone and their relation to gas hydrate stability, *Geology*, *26*, 647-650.

Chand, S., T. A. Minshull, D. Gei, and J. M. Carcione (2004), Elastic velocity models for gas-hydrate-bearing sediments - a comparison, *Geophysical Journal International*, *159*(2), 573-590.

Collett, T., M. Riedel, J. Cochran, R. Boswell, J. Presley, P. Kumar, A. Sathe, A. Sethi, M. V. Lall, and V. Sibal (2006), Expedition 01 Initial Reports*Rep.*

Cook, A. E., D. Goldberg, and R. L. Kleinberg (2008), Fracture-controlled gas hydrate systems in the northern Gulf of Mexico, *Marine and Petroleum Geology*, *25*(9), 932-941.

Dai, J. C., F. Snyder, D. Gillespie, A. Koesoemadinata, and N. Dutta (2008), Exploration for gas hydrates in the deepwater, northern Gulf of Mexico: Part I. A seismic approach based on geologic model, inversion, and rock physics principles, *Marine and Petroleum Geology*, *25*(9), 830-844.

Daigle, H., and B. Dugan (2010), Origin and evolution of fracture-hosted methane hydrate deposits, *Journal of Geophysical Research-Solid Earth*, *115*.

Dvorkin, J., and A. Nur (1996), Elasticity of high-porosity sandstones: Theory for two North Sea data sets, *Geophysics*, *61*(5), 1363-1370.

Gassmann, F. (1951), Elastic Waves Through A Packing Of Spheres, *Geophysics*, *16*(4), 673-685.

Hashin, Z., and S. Shtrikman (1963), A variational approach to the theory of the elastic behaviour of multiphase materials, *Journal of the Mechanics and Physics of Solids*, *11*(2), 127-140.

Helgerud, M. B., J. Dvorkin, and A. Nur (2000), Rock physics characterization for gas hydrate reservoirs - Elastic properties, in *Gas Hydrates: Challenges for the Future*, edited by G. D. Holder and P. R. Bishnoi, pp. 116-125.

Helgerud, M. B., J. Dvorkin, A. Nur, A. Sakai, and T. Collett (1999), Elastic-wave velocity in marine sediments with gas hydrates: Effective medium modeling, *Geophysical Research Letters*, *26*(13), 2021-2024.

Jakobsen, M., T. A. Johansen, and B. O. Ruud (2001), Modeled velocity and reflectivity properties of anisotropic hydrated sediments, *Journal of Computational Acoustics*, *9*(4), 1507-1522.

Jakobsen, M., J. A. Hudson, T. A. Minshull, and S. C. Singh (2000), Elastic properties of hydrate-bearing sediments using effective medium theory, *Journal of Geophysical Research-Solid Earth*, *105*(B1), 561-577.

Kida, M., K. Suzuki, T. Kawamura, H. Oyama, J. Nagao, T. Ebinuma, H. Narita, H. Suzuki, H. Sakagami, and N. Takahashi (2009), Characteristics of Natural Gas Hydrates Occurring in Pore-Spaces of Marine Sediments Collected from the Eastern Nankai Trough, off Japan, *Energy & Fuels*, *23*(11), 5580-5586.

Kvenvolden, K. A. (1994), Natural Gas Hydrate Occurrence and Issues, *Annals of the New York Academy of Sciences*, *715*, 236-242.

Priest, J. A., E. V. L. Rees, and C. R. I. Clayton (2009), Influence of gas hydrate morphology on the seismic velocities of sands, *Journal of Geophysical Research-Solid Earth*, *114*.

Sava, D., and B. Hardage (2010), Rock-physics models for gas-hydrate systems associated with unconsolidated marine sediments, in *Natural Gas Hydrates - Energy Resource and Associated Geologic Hazards*, edited by T. Collett, A. Johnson, C. Knapp and R. Boswell, The American Association of Petroleum Geologists, Vancouver, Canada.

Winters, W. J., I. A. Pecher, W. F. Waite, and D. H. Mason (2004), Physical properties and rock physics models of sediment containing natural and laboratory-formed methane gas hydrate, *American Mineralogist*, *89*(8-9), 1221-1227.

VITA

Samiya AbdulRahman Al-Bulushi

Candidate for the Degree of

Master of Science

Thesis: QUANTIFICATION OF GAS HYDRATES IN FRACTURED MARINE SEDIMENTS, KRISHNA GODAVARI BASIN, INDIA

Major Field: Geology

Biographical:

Education:

Bachelor of Science in Petroleum Engineering, Sultan Qaboos University, Muscat, Oman, 2009.

Completed the requirements for the Master of Science in Geology at Oklahoma State University, Stillwater, Oklahoma in May,2012.

Experience:

Professional Memberships:
Honor Society of Phi Kappa Phi
American Association of Petroleum Geologists (AAPG)

Name: Samiya Al-Bulushi Date of Degree: May,2012

Institution: Oklahoma State University Location: Stillwater, Oklahoma

Title of Study: QUANTIFICATION OF GAS HYDRATES IN FRACTURED MARINE SEDIMENTS, KRISHNA GODAVARI BASIN, INDIA

Pages in Study: 27 Candidate for the Degree of Master of Science

Major Field: Geology

Scope and Method of Study:

An effective medium theory for modeling elastic velocities in unconsolidated sediments with hydrate-saturated, random fractures was developed. In this model, elastic velocities are not sensitive to the size or orientation of fractures but only to their density and interconnectivity (the two extreme cases being fully disconnected and fully connected fractures).

Findings and Conclusions:

Comparing hydrates in fractures with other familiar states of hydrates suggest that elastic velocities increase due to hydrate-saturated fractures are more rapid than hydrates in pore-filling and load-bearing states. However, the increment is dependent on the mode of fractures; interconnected fractures show the highest velocity response. In Krishna Godavari (KG) Basin at NGHP 01-10 site, V_P, V_S, and hydrate saturation can be explained by simultaneously assuming two growth styles of hydrates– in matrix as load-bearing phase as well as in fractures. Although occurrence of fractures; both connected and disconnected show high fractures hydrates saturation (above 50% of fractures porosity), these zones are also associated with background matrix of low hydrates saturations and overall less total saturations.

ADVISER'S APPROVAL: Priyank Jaiswal